Analysis of adiabatic shear banding in orthogonal cutting of Ti alloy

M.H. Miguélez [a,*], X. Soldani [a], A. Molinari [a,b]

[a] Department of Mechanical Engineering, Universidad Carlos III de Madrid, Avda. Universidad 30, 28911 Leganés, Madrid, Spain
[b] Laboratoire d'Etude des Microstructures et de Mécanique des Matériaux, LEM3, Labex Damas, Université de Lorraine, Ile du Saulcy, Metz Cedex, France

Abstract: This work is focused on the numerical analysis of adiabatic shear banding in orthogonal cutting of Ti6Al4V alloy. Segmented chip results from adiabatic shear banding, depending on the competition of thermal softening and strain and strain rate hardening. The influence of cutting velocity and feed in the chip segmentation is studied. Also the role of friction at the tool-chip interface and the effect of rheological parameters of the constitutive equation are analyzed. Experimental tests obtained from previous work of the authors [Molinari A, Musquar C, Sutter G, Adiabatic shear banding in high speed machining of Ti–6Al–4V experiments and modeling, Int J Plast, vol. 18, 2002, p. 443–459] and others were used as a reference to validate the models. Cutting forces and the mechanism of plastic flow localization are analyzed in terms of frequency of segmentation and shear band width and compared to experimental data.

Keywords: Adiabatic shear banding, Ti6Al4V, Numerical modeling, Orthogonal cutting Chip, segmentation

1. Introduction

Thermo-resistant alloys such as Ti alloys and nickel-based alloys are widely used in high responsibility applications, for instance in aero engine components, due to high corrosion strength and good mechanical properties at high temperature. Mechanical properties of these alloys and their low thermal conductivity are related with low machinability during cutting processes. High temperatures are produced at the interface resulting in reduced tool life and could also affect surface integrity of the workpiece [1].

Finite element (FE) method has been widely used to model metal cutting and to improve the understanding of mechanisms of chip generation, contact phenomena [2] and the effect in surface integrity [3]. This approach allows gathering information on difficult to measure variables during the machining process. High speed cutting of thermo-resistant alloys commonly produces serrated and segmented chip due to adiabatic shear banding at the primary shear zone. Numerical models should be able to reproduce localization phenomena [4].

The interest for industrial applications of Ti alloys, has motivated a great number of scientific works focusing on machining of these materials. The alloy Ti6Al4V is commonly used in a variety of structural engineering applications and has been considered as one of the best examples to study chip segmentation [5].

* Corresponding author. Tel.: +34 916 2494 02.
E-mail address: mhmiguel@ing.uc3m.es (M.H. Miguélez).

Molinari et al. [6] presented an experimental analysis of orthogonal cutting of a Ti6Al4V ranging from 0.01 to 73 m/s using a high-speed testing machine and a ballistic set-up. The shear band width and the distance between bands were determined by micrographic observations, analyzing their dependence upon cutting velocity and feed.

Sun et al. [7] experimentally analyzed chip formation during dry turning of Ti6Al4V alloy under different cutting speeds, feed rates and depths of cut. High frequency of the cyclic force was caused by the segmented chip formation process. The frequency of segmentation was found to be proportional to the cutting speed and inversely proportional to the feed rate. Similar behavior was observed by Cotterell and Byrne [8] using image analysis of the recorded video sequences.

Some processing routes vary the elastic limit or the strain hardening capacity of the material. Analyzing how machining operations are affected by values of material parameters is a prerequisite for understanding the effects of material processing prior to machining. The influence of material behavior on the formation of shear bands in cutting has been analyzed by different authors with Finite Element modeling. Umbrello [9] analyzed the effect of plastic flow parameters on the cutting process of TiAl6V4 alloy. The Johnson–Cook's constitutive equation (with three different sets of material constants) was implemented in a numerical machining model and the results were compared with experimental data, establishing that fairly good numerical results could be obtained. Naturally, the goodness of results is only insured for cutting conditions for which the loading rates and stresses undergone by the work-material are in the range explored during the

experimental characterization of the work-material constitutive law as shown for instance by Muñoz-Sanchez et al. [10].

Calamaz et al. [11] implemented a new material constitutive law in a 2D finite element model to analyze the chip formation and shear localization when machining titanium alloys. The model accounted for the influence of strain, strain rate and temperature on the flow stress and also introduced a strain softening effect. The hypothesis of a material strain softening phenomenon enables prediction of a segmented chip under low cutting speeds and feeds. The influence of strain softening on chip generation and the evolution of temperature and cutting forces, have been also analyzed in the work of Sima and Özel [12]. It was found that flow softening increases the degree of chip serration producing more curved chips.

Karpat [13] proposed various temperature-dependent flow softening scenarios which were tested using finite element simulations. The results were compared with experimental data from the literature: flow softening initiating around 350–500 °C combined with appropriate softening parameters yields simulation outputs in good agreement with the experimental measurements.

Chen et al. [14] analyzed with a FE code the distribution of stresses, temperature, and strains during the process of chip segmentation in orthogonal cutting. It was shown that thermal softening predominates over strain hardening along adiabatic shear band during segmented chip formation while strain hardening predominates over thermal softening between two adjacent shear bands

Bäker et al. [15] and Bäker [16], developed a two dimensional finite element model of orthogonal cutting process and analyzed the influence of material parameters on cutting forces and on the chip formation. General trends concerning chip segmentation were deduced related with workpiece material behavior: the tendency to chip segmentation should be enhanced in materials with greater strength; materials with small yield strength and a large amount of hardening should show a transition to segmented chips only at very high cutting speeds or not at all; materials in which strong strain softening occurs should form segmented chips at all cutting speeds.

Bäker et al. [17] studied the influence of thermal conductivity on the chip segmentation process. Increase in thermal conductiv-ity leads to a decreasing degree of segmentation and increasing in the cutting force, showing the importance of heat localization in the formation of segmented chips.

The current demands of productivity and workpiece quality have led to the increase of cutting speed even in the case of difficult to cut materials. Despite of the efforts developed in the study of machining of Ti alloys the understanding of the thermo-mechanical phenomenon involved during cutting is still an important objective.

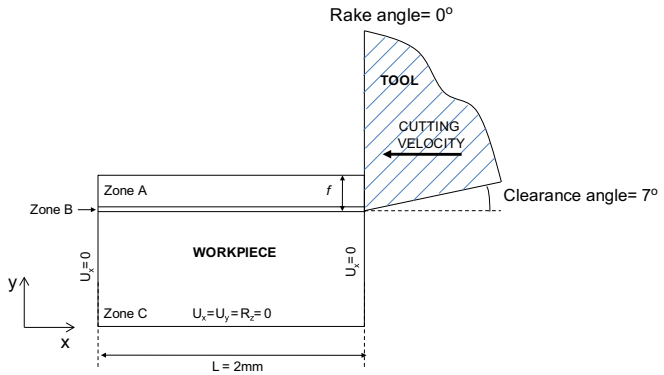

Fig. 1. Scheme of the numerical model including boundary conditions (U displacement, R rotation).

In this paper, we perform numerical simulations of orthogonal cutting of Ti6Al4V in a wide range of cutting speeds and feed rates in order to investigate the phenomena involved during chip segmentation. A finite element model is developed and validated in terms of cutting forces, frequency of segmentation and chip morphology by comparison with experimental results obtained from literature including previous work of the authors [6]. The dependence of cutting forces and chip morphology with respect to cutting parameters, friction coefficient and material rheological parameters is analyzed. The paper is organized as follows. The numerical model is described in the second section. In third section cutting forces and overall friction coefficient are analyzed while chip morphology is presented in sections fourth and fifth. Main contributions of the paper are summarized in the conclusions.

2. Numerical modeling

As it has been commented in the previous section, Finite Element (FE) modeling of cutting processes has been widely used to improve the understanding of mechanisms of chip generation. Numerical simulations permit to gather information on difficult to measure variables during machining processes and also diminish the need of experimental work which is commonly time consuming and expensive. These approaches have been used for decades focusing on different aspects of the metal cutting process such as, interface contact [2,18], constitutive model of the workpiece [19], surface integrity [3] or influence of tool wear [20]. The simulation of oblique cutting commonly performed in real industrial applications needs three dimensional (3D) modeling. The detail of the tool nose and cutting surfaces geometry can only be reproduced with three dimensional approaches. However two dimensional (2D) models of orthogonal cutting, widely used in the scientific literature, are very useful to simulate phenomena such as adiabatic shearing at the primary shear zone (being the objective of this paper) or contact phenomena at the secondary zone (see for instance, previous works of the authors [2,21]). Moreover a very fine mesh is required in order to predict shear band width; this fact increases computational cost and makes really difficult the use of 3D models involving very large number of elements and long calculation time.

Thus 2D approach has been used in this work in order to model orthogonal cutting of Ti alloy. A plane strain model was developed using the commercial Finite Element code ABAQUS/Explicit with Lagrangian formulation. A thermo-mechanical coupled analysis was developed by using CPE4RT element type [22]. Those are plane strain, quadrilateral, linearly interpolated, and thermally coupled elements with reduced integration and automatic hour-glass control.

The basic geometry, dimensions and boundary conditions of the numerical model are shown in Fig. 1. The workpiece is fixed in some contours and the cutting speed is applied to the tool. Plane strain condition is assumed. In this study the rake angle is zero.

The workpiece is divided into three different zones where the mesh has different characteristics. The layer of material which will be removed by cutting is composed of Zone A (main part) and Zone B (thin bottom layer of 4 μm thick). The upper limit of Zone C corresponds to the machined surface. The mesh at Zone B and C is parallel to horizontal and vertical directions, while the mesh at the Zone A is characterized by an inclination angle θ with the horizontal direction. The aim of this mesh configuration is to facilitate the formation of segmented chip during machining of Ti alloys [4]. As occurs in other localization problems the formation of adiabatic band is easier when the mesh is oriented parallel to the band. Thus the inclination angle of the mesh should be close to

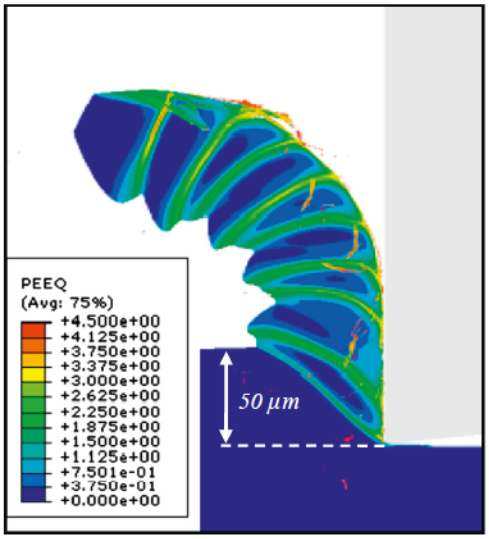

Fig. 2. Formation of shear bands: equivalent plastic strain contours obtained during formation of segmented chip (cutting speed 6 m/s, feed 50 microns, friction coefficient = 0.4).

the direction of shear banding. Formation of shear bands is illustrated in Fig. 2 where the field of equivalent Mises plastic deformation has been displayed.

The sensibility of the model to the element size was checked by comparing results obtained with different values of element size (1, 2 and 6 μm). The smallest element size (1 μm) was used to get sufficient accuracy in the results.

Also the influence of mesh inclination θ was analyzed. The value was stated equal to 40° but other mesh configurations with θ equal to 35°, 45°, and 50° were also considered. Only small variations in terms of chip frequency were observed (around 8%) while the rest of parameters did not change significantly.

There are different possibilities for selecting an erosion criterion for highly distorted elements elimination when simulating mechanical processes involving elevated strain, such as machining or impact problems for instance. Analysis and calibration of seven fracture models such as constant equivalent strain, maximum shear stress or Johnson–Cook fracture model can be found in [23].

In this paper a simple erosion criterion was stated as the maximum level of the equivalent plastic strain ε_p^{crit} above which mesh elements are erased. This criterion available in most commercial FE codes has been widely used for simulation of chip separation. It should be fixed in a range representative of mechanical phenomena involved during cutting. It is recommendable to select a higher value in the primary zone than that imposed at the zone of separation line due to the different values of triaxiality between both zones. At the separation zone and for the zero value of the rake angle considered here, the material is subjected to positive values of triaxiality just before rupture. However, the combination of compressive and shear loading exerted at the primary zone leads to negative or small values of triaxiality. It is accepted that the level of rupture deformation is lower as the triaxiality increases [23]. The level of ε_p^{crit} have been stated equal to 4 in both Zones A and C (in order to remove just few highly distorted elements, most elements remained active in the model), and equal to 3 in Zone B. The erosion criterion is not critical in Zone C since most of the elements experiences low deformation far from erosion values, only few element at the beginning of the calculation are distorted and the erosion is applied in order to avoid calculation ending. The value $\varepsilon_p^{crit} = 3$ is close to those used when modeling material failure at high strain rates such as in ring expansion experiments [24]. The geometrical and numerical

Table 1
Parameters of constitutive equation for Ti alloy used in simulations [26].

	A (MPa)	B (MPa)	n	C	m	$\dot{\varepsilon}_0$(1/s)
Ti6Al4V	782	498	0.28	0.028	1.0	10^{-5}

Table 2
Physical properties of Ti6Al4V from website AZOM, 2013.

Density (kg/m^3)	4420
Thermal conductivity (W/m K)	7.2
Specific heat capacity (J/kg K)	560
Thermal expansion (1/K)	9.2×10^{-6}
Modulus of elasticity (GPa)	114

characteristics of the model allow for performing simulations of orthogonal cutting in a large range of cutting speeds. Interruption of calculations due to excessive mesh distortion could be avoided.

It should be noted that in the present modeling the separation of the chip from the workpiece occurs by deletion of a layer of elements along the workpiece surface. Let us denote by G_c the energy consumed by the separation process per unit machined surface. As the separation process is similar to mode 1 ductile crack propagation, G_c is related to the fracture toughness K_{Ic} by the relationship $G_c = (K_{Ic}^2/2E)$, where E is the Young elastic modulus. For a titanium alloy with $K_{Ic} = 60$ MPa m$^{1/2}$ and $E = 100$ GPa, we have $G_c = 18{,}000\ J/m^2$. It is checked in Appendix A that: (i) for titanium alloys and for the values of the feed considered here, the separation energy is small as compared to the total cutting energy, (ii) the separation energy involved in the present model is comparable to the theoretical value $G_c = 18{,}000\ J/m^2$. However, there is no need in the numerical model to return precisely the theoretical value $G_c = 18{,}000\ J/m^2$ since in any case the separation energy is playing a minor role in our problem.

The tool was assumed to be rigid. The workpiece material was taken to be elastic–viscoplastic, isotropic, and to obey the J_2 flow theory (Mises yield criterion). The viscoplastic constitutive response was described by the Johnson–Cook law [25]

$$\sigma_Y = (A + B\varepsilon_p^n)\left(1 + C\ln\frac{\dot{\varepsilon}_p}{\dot{\varepsilon}_0}\right)\left(1 - \left(\frac{T - T_0}{T_m - T_0}\right)^m\right) \quad (1)$$

where σ_Y is the tensile flow stress, ε_p is the accumulated plastic strain, $\dot{\varepsilon}_p$ is the equivalent Mises plastic strain rate and T is the absolute temperature. For Ti6Al4V alloy, the parameters of the constitutive equation were obtained from [26] and are shown in Table 1. Table 2 summarizes the physical properties of Ti6Al4V obtained from the website AZOM [27].

Concerning heat generation due to plastic work the value of the Quinney–Taylor coefficient was taken as $\beta = 0.9$. The initial temperature T_0 for both the tool and the workpiece was equal to 293 K, the melting temperature was 1900 K.

The contact at the tool-chip interface is simulated with the simple Coulomb law. Constant values of the friction coefficient are assumed (ranging from 0 to 0.8). The ability of this formulation to reproduce complex phenomena including sticking at the tool-chip interface due to thermal softening has been shown in a previous work of the authors [21].

3. Cutting forces and overall friction coefficient

Fig. 3a shows the evolution with time of the specific cutting force $F_C/(bf)$ (b is the width of cut and f is the feed, see Fig. 1) for the low cutting speed V=1 m/s (continuous chip) and the high

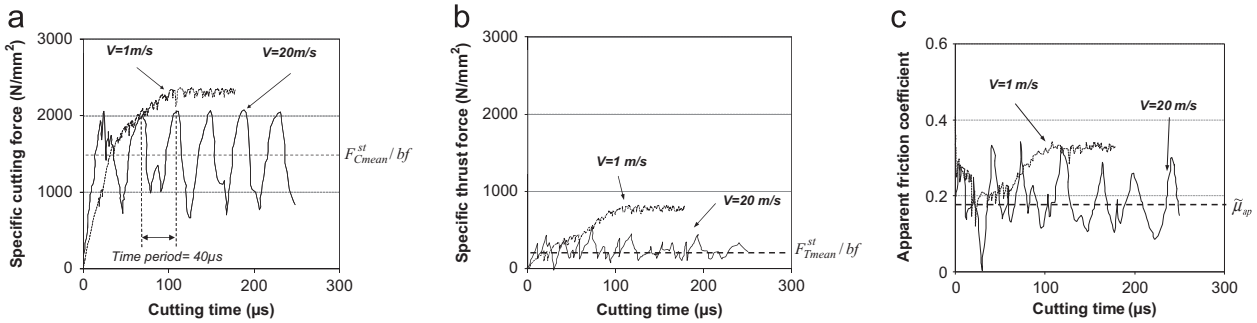

Fig. 3. Evolution with time of (a) the specific cutting force, (b) the specific thrust force and (c) the overall friction coefficient. Low and high cutting speeds are considered (respectively 1 and 20 m/s), corresponding to continuous and segmented chip. The feed is 100 microns and the sliding friction coefficient is 0.4.

speed $V=20$ m/s (segmented chip). In the case of continuous chip formation ($V=1$ m/s), after a transient regime of about 0.1 ms, the cutting force reaches a stationary value which is denoted as F_C^{st}.

For $V=20$ m/s, chip segmentation occurs and a steady state periodic regime is rapidly realized after about 0.07 ms. In the steady state regime the cutting force has periodic oscillations with a well defined time period. Each drop of the force coincides with the formation of an adiabatic shear band. Adiabatic shearing is the consequence of thermal softening which triggers instability of the plastic flow. The mean cutting force F^{st}_{Cmean} is defined as the time average of the force over several time periods. The associated specific cutting force is $F^{st}_{Cmean}/(bf)$, see Fig. 3a.

Fig. 3b shows the evolution with time of the specific thrust force $F_T/(bf)$ for low and high cutting speeds. When periodic oscillations occur, the mean specific thrust force $F^{st}_{Tmean}/(bf)$ is defined as was done for the cutting force. Identical trends are observed in Fig. 3a and b.

The apparent friction coefficient is defined as the ratio between thrust and cutting force $\mu_{ap}=(F_T/F_C)$. The evolution of μ_{ap} with time is shown in Fig. 3c for low and large values of the cutting speed. Oscillations are seen when segmentation occurs. Then, a time average value $\tilde{\mu}_{ap}$ is defined in the steady regime, see Fig. 3c.

Cutting forces obtained with the model are compared in Fig. 4 to experimental results referring to orthogonal cutting of Ti6Al4V alloy. The characteristics of these experimental works are briefly described in the following.

Molinari et al. [6] analyzed the development of adiabatic shear banding on a wide range of cutting speeds (from 0.01 m/s to 73 m/s) in orthogonal cutting with a tool with rake angle equal to zero. Two devices were used for the experimental tests. A universal high-speed testing machine for the low cutting speeds (from 0.01 to 1 m/s). The highest velocities (from 10 to 73 m/s) were achieved with an airgun set-up. In both cases, the cutting force was measured for two values of the feed (120 and 250 μm). The authors studied the chip morphology: frequency of segmentation and width of shear band.

Armendia et al. [28] measured the cutting forces in orthogonal cutting process for feed 100 μm and depth of cut 2 mm. Cutting velocity ranged from 0.83 to 1.5 m/s. The clearance angle of the tool was equal to 6°, and the rake angle was equal to 7°.

Cotterell and Byrne [29], performed experimental tests in orthogonal cutting conditions (rake angle equal to 6.5°) and cutting velocity ranging from 0.067 to 2 m/s. Cutting forces, temperature distribution, tool-chip contact length and the shear angle, were obtained for different values of the feed (50, 75 and 100 μm).

Fang and Wu [30] studied high speed finishing operation in which the tool edge radius plays a significant role. The tool chosen in the experiments was cemented carbide with a TiC/TiN/TiCN coating with rake angle 5° and edge radius 60 μm. The authors have limited the study to low velocity (from 0.97 to 2.9 m/s) and four values of the feed (75, 90, 105 and 120 μm). The large value of the ratio between edge radius and feed led to high specific cutting forces, the highest between the cases reviewed.

Hoffmeister [31] and Gente and Hoffmeister [32], studied the chip formation of Ti6Al4V in orthogonal cutting in a wide range of cutting speed from 5 m/s to 100 m/s. The cutting experiments were performed with two values of the uncut chip thickness (40 and 80 μm) and two rake angles (0° and 30°). The width of cut was 5 mm.

Fig. 4a and b shows the evolution of the specific cutting and thrust forces in terms of the cutting speed. Considering specific forces allows for comparing results at different values of the feed (in the interval 80–127 microns).

Various values of the sliding friction coefficient μ (ranging from 0 to 0.8) are accounted. For discontinuous chip the mean stationary values of the cutting and feed forces are considered, respectively (F^{st}_{Cmean}/fb) and (F^{st}_{Tmean}/fb).

We note that, in agreement with [21], the effect of μ is getting negligible at high cutting speeds and for $\mu\geq 0.4$ due to the sticking of the chip to the tool generated by the enhanced thermal softening.

Fig. 4a and b show that the correlation of the modeling with experimental data is rather satisfactory. The variability in experimental data between the various works considered may be due to differences in the cutting tools and to different thermomechanical histories experienced by the Ti alloys during their manufacture.

The influence of cutting speed on cutting and thrust forces could be summarized in two aspects. At relatively low cutting speed (lower than 5 m/s) a large decrease of the cutting force with the velocity is observed. At higher cutting speeds the value of cutting force tends to saturate and no significant force drop is seen when the cutting speed is increased.

Fig. 4c shows the dependence of the average apparent friction coefficient $\tilde{\mu}_{ap}$ with respect to the cutting speed for various values of the sliding friction coefficient μ (entering into the Coulomb friction law). It is seen that $\tilde{\mu}_{ap}$ decreases significantly with the cutting speed for large values of the sliding friction coefficient ($\mu\geq 0.4$). The apparent friction coefficient follows trends similar to those of the thrust force displayed in Fig. 4b. These trends have been discussed in [21] and are essentially related to the higher contribution of sticking at the tool chip interface when the cutting speed is increased. The expansion of the sticking zone is a consequence of thermal softening of the work-material along the rake face. For $\mu\geq 0.4$ and at high cutting speeds the tool-chip contact is mostly governed by the shear flow stress of the work material along the sticking zone and the contribution of the sliding friction coefficient μ to the apparent friction coefficient becomes negligible. This feature is clearly seen in Fig. 4c.

On the contrary, for low values of μ the tool-chip contact is mostly governed by sliding friction, and the effect of μ on the apparent friction coefficient $\tilde{\mu}_{ap}$ remains significant at high cutting speeds.

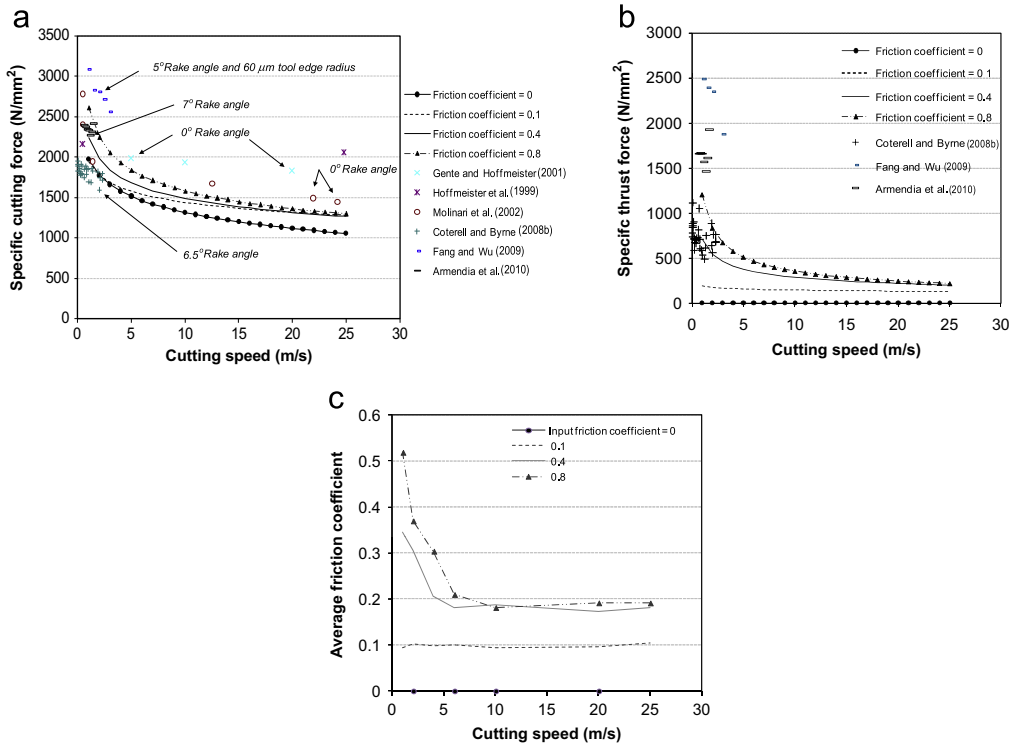

Fig. 4. Evolution with cutting speed of the (time averaged): (a) specific cutting force $F^{st}_{Cmean}/(bf)$, (b) specific thrust force $F^{st}_{Tmean}/(bf)$ and (c) apparent friction coefficient $\tilde{\mu}_{ap}$. Numerical results are compared to experimental data from literature.

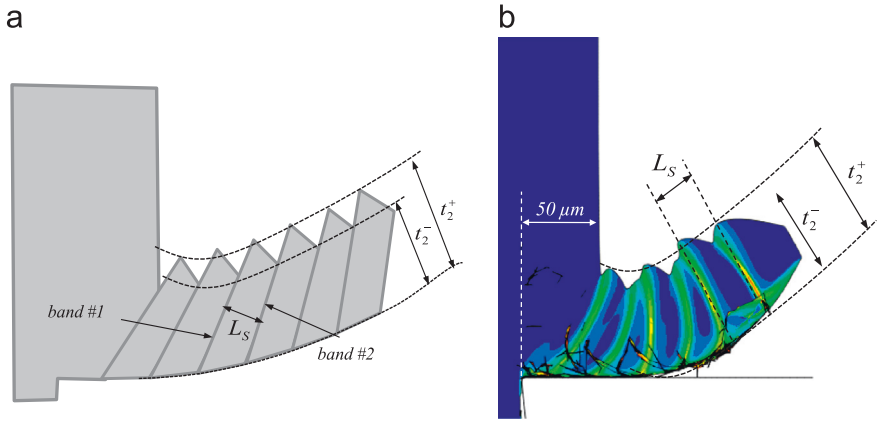

Fig. 5. Characterization of chip segmentation : L_s is the mean shear band spacing; t_2^+ and t_2^- are the peak and valley levels respectively. (a) schematic view of a regular chip and (b) irregular chip morphology obtained for feed 50 microns and cutting speed 6 m/s. In this case average values of L_s, t_2^+ and t_2^-, and along the chip are considered.

4. Chip morphology: effect of cutting velocity and feed

4.1. Characterization of chip serration

The parameters used to characterize chip serration are presented in Fig. 5. The mean thickness of the deformed chip ($\bar{t}_2$) is obtained as $\bar{t}_2 = (t_2^- + t_2^+)/2$.

t_2^+ and t_2^- represent respectively the level of peaks and valleys with respect to the base of the chip, see Fig. 5a. The shear band spacing L_s is the distance between two consecutive bands. If the chip morphology is irregular as in Fig. 5b, t_2^+, t_2^- and L_s are meant as average values along the chip.

The evolution of t_2^+ and t_2^- with the cutting speed V is shown in Fig. 6 for the feed f=100 microns. A transition from continuous to serrated chip is observed and the evolution of t_2^+ and t_2^- is rapid in the range of relatively low cutting speed (< 5 m/s). At higher velocities the values of t_2^+ and t_2^- do not experience significant changes.

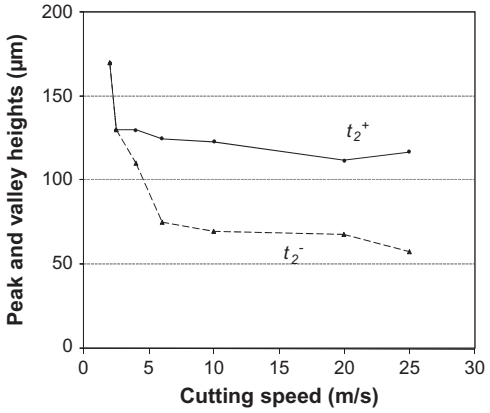

Fig. 6. Evolution of peak and valley levels, respectivel t_2^+ and t_2^-, with cutting speed (feed 100 microns and sliding friction coefficient 0.4).

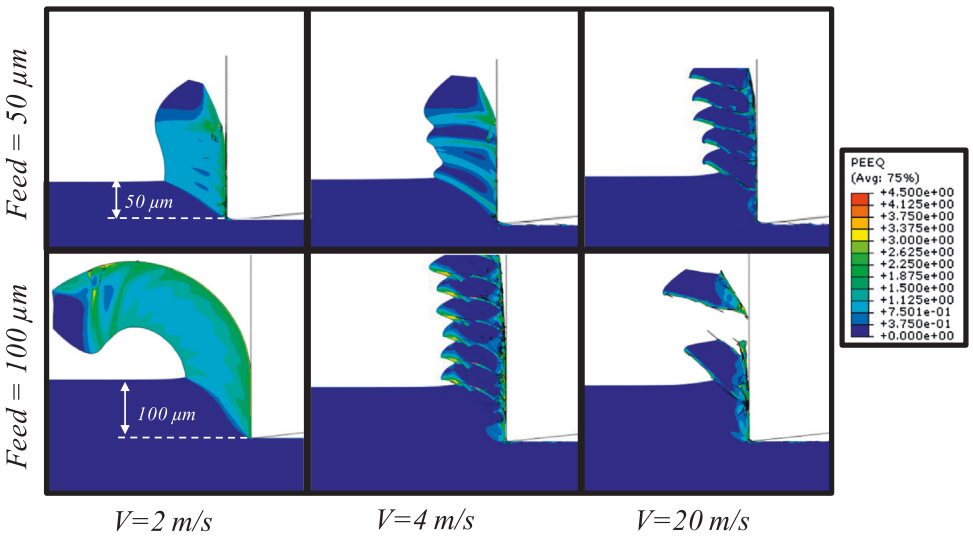

Fig. 7. Evolution of the chip morphology of Ti6Al4V alloy with the cutting speed (sliding friction coefficient 0.1; feed 50 and 100 microns). Equivalent plastic strain level contours are shown.

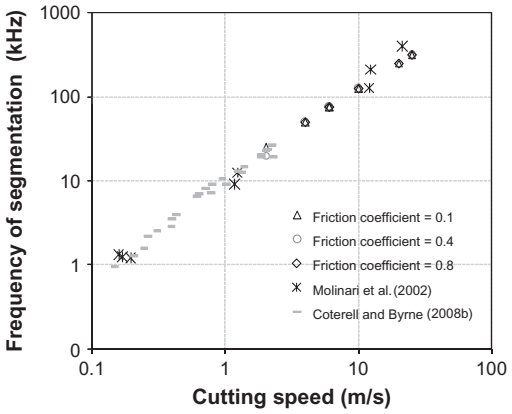

Fig. 8. Influence of the cutting speed and of the sliding friction coefficient on the frequency of segmentation. Simulations are performed with the feed of $f=0.1$ mm and a sharp tool. Experimental data of Molinari et al. [6] and of Cotterell and Byrne [8] are performed with $f=120$ microns and $f=100$ microns, respectively.

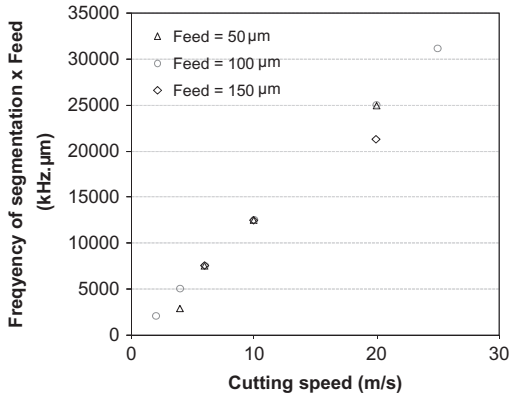

Fig. 9. Frequency of segmentation multiplied by the feed f vs cutting speed (simulation results). The frequency of segmentation appears to be proportional to the cutting speed and inversely proportional to the feed.

The evolution of the chip morphology with cutting speed is illustrated in Fig. 7 for the feeds 50–100 microns. Continuous chip formation is observed at low cutting speed (2 m/s). Adiabatic shearing appears between 2 m/s and 4 m/s. As the cutting speed increases, the trend to segmentation is enhanced and at high cutting speed the chip is completely segmented. In the experiments by Molinari et al. [6] saw-tooth chip was observed for cutting speeds, V, lower than 1.2 m/s while continuous chip formation is predicted by the present simulations for these low cutting speeds. However, for $V<1.2$ m/s the experiments did not show evidence of well formed shear band. The shear band width which was clearly defined at larger cutting speeds (>13 m/s) could not be measured at $V<1.2$ m/s. Adiabatic heating and possibly phase transformation are activated at high cutting speeds. At lower cutting speeds, dynamic recrystallization might be involved in the mechanism of shear flow instability [33]. The material softening due to dynamic recrystallization of Ti6Al4V is not simulated with the present FE model.

4.2. *Frequency of segmentation and shear band spacing*

The frequency of segmentation (the inverse of the time interval between two consecutive drops of the cutting force) is illustrated in Fig. 8, together with experimental results obtained for Ti 6Al4V by Molinari et al. [6] and Cotterell and Byrne [29]. The frequency of segmentation exhibits a linear dependence with cutting speed V (logarithmic scale) for $V>1$ m/s. There is no friction dependence of the frequency of segmentation (four values of the sliding friction coefficient were considered, 0, 0.1, 0.4 and 0.8).

The influence of the feed f is illustrated in Fig. 9, showing the frequency of segmentation multiplied by the feed, for: $f=50$, 100 and 150 microns. The segmentation frequency varies linearly with the cutting speed irrespective of the feed considered. From the results shown in Fig. 9, it appears that the frequency of segmentation is inversely proportional to the feed. It will be shown later that this feature is due to the fact that the shear band spacing L_s is proportional to the feed in the range of cutting speeds considered here.

Fig. 10a and b provides the band spacing L_s as a function of the cutting speed. These results were deduced from chip morphologies obtained with numerical simulations as those displayed in Fig. 7.

Fig. 10a indicates that the band spacing is approximately constant with respect to the cutting speed (in the range of velocities explored here). This trend is in agreement with experimental results obtained by Calamaz et al. [11], Sun et al. [7], Sima and Özel [12] and Ye et al. [34] which are presented together with numerical results in Fig. 10a.

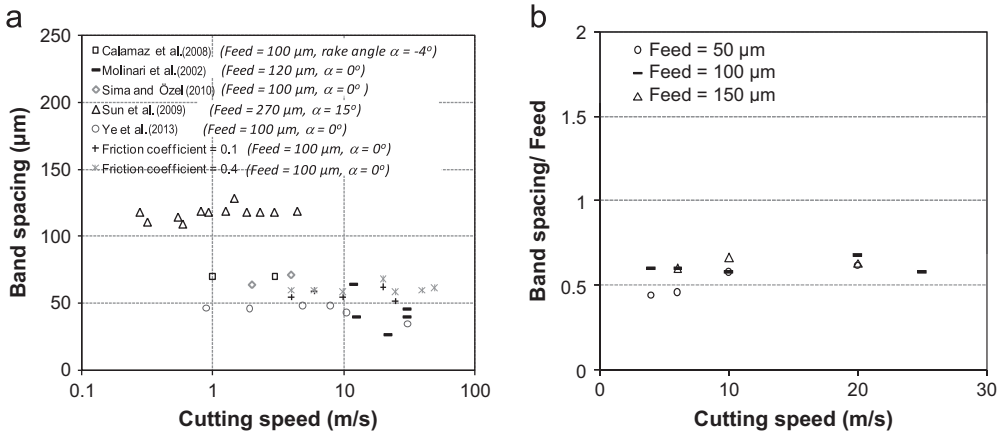

Fig. 10. (a) Influence of the cutting speed V on the band spacing L_s. Numerical simulations are performed with a sharp tool and the feed 100 microns. Experimental data are obtained at various feeds and cutting edge radii. For a given feed f, L_s appears as independent of V (in the range of cutting speeds considered here) and (b) L_s/f in terms of V. It appears that the band spacing L_s is nearly proportional to the feed. The value of the friction coefficient is 0.4.

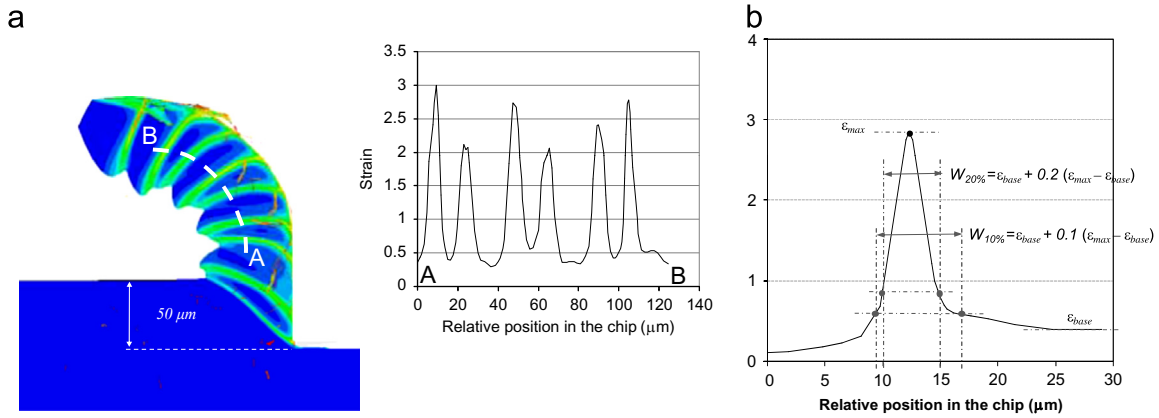

Fig. 11. (a) Distribution of the equivalent plastic strain in the chip (left) and along the path AB (dashed line). Cutting conditions are V=6 m/s and f=50 microns and the friction coefficient is 0.4 and (b) Schematic view showing the definition of $w_{20\%}$.

From the theoretical and numerical results displayed in Fig. 10a it appears that the shear band spacing L_s is proportional to the feed. This is clearly confirmed by Fig. 10b showing L_s/f in terms of the cutting speed for various values of the feed.

It should be noted that the agreement between theoretical predictions and experimental data in Fig. 10a is satisfactory despite slight variations in experimental configurations. Variations in cutting angles of the inserts could influence the results shown in Fig. 10a. Molinari et al. [6], Sima and Ozel [12] and Ye et al. [34] used a null rake angle. For Sun et al. [7] and Calamaz et al. [11] the rake angle was equal to 15° and −4°, respectively. It is worth mentioning that, according to Atlati et al. [35] the shear band spacing increases when the rake angle α is reduced. Thus, for a zero rake angle the values of L_s of Calamaz et al. [11] shown in Fig. 10a would be lowered and therefore would be in better agreement with the results of the simulations made for α=0 and other experimental results also obtained for α=0.

The results could be also affected by different tool edge radii. To check this effect, some simulations have been performed with a tool edge radius of 25 µm and compared to results obtained with a sharp tool. It was observed that the shear band spacing increases with the edge radius. However this effect is moderate and does not compromise the good correlation observed in Fig. 10a between theoretical and experimental results.

The fact that the shear band spacing is independent from cutting speed and proportional to the feed (see Fig. 10b showing the ratio band spacing over feed versus cutting speed) leads to a segmentation frequency that is proportional to the cutting speed and inversely proportional to the feed as observed in Fig. 9.

4.3. Shear band width

Few authors have theoretically analyzed the thickness of adiabatic shear bands occurring during cutting operations. Thus, a procedure to characterize the shear band width from numerical simulations should be firstly developed. In this work the shear band width is measured from strain fields. The interest of using a strain measurement in place of strain rate comes from the fact that, during the cutting process, the strain profile associated to a shear band remains unaltered as soon as the band is formed. Typical strain profiles along a line perpendicular to shear bands are displayed in Fig. 11a.

The shear band width cannot be defined in an absolute way. However, an operational way to characterize the width of a shear band can be developed as follows. For a given band, consider the peak strain ε_{max} accumulated in the band and define by ε_{base} the strain level outside the band, see Fig. 11b. We define $w_{20\%}$ as being the width of the shear zone where the strain is higher than the reference strain level $\varepsilon_{base}+0.2(\varepsilon_{max}-\varepsilon_{base})$, see Fig. 11b (20% refers to the factor 0.2 in this relationship). $w_{20\%}$ represents somehow an arbitrary definition of the shear band width, but this definition is sufficient to analyze trends, i.e. the effects of loading conditions on the distribution and intensity of shear localization. The definition $w_{10\%}$ corresponding to strains higher than $\varepsilon_{base}+0.1(\varepsilon_{max}-\varepsilon_{base})$ will be also used in order to show the consistency of results when

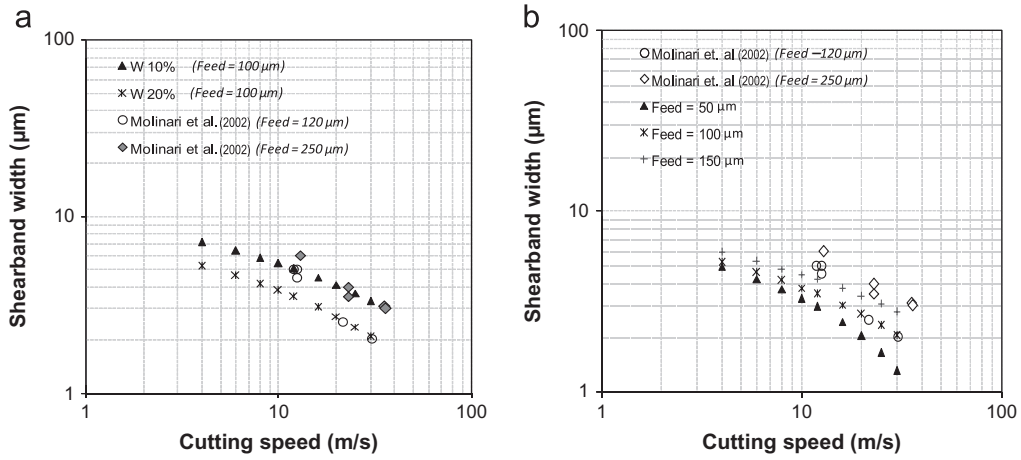

Fig. 12. (a) Evolution of the shear band width with the cutting speed. Numerical results, based on the definitions $w_{10\%}$ and $w_{20\%}$ of the shear band width, are compared to experimental data of Molinari et al. [6] and (b) numerical results based on $w_{20\%}$ for several values of the feed, compared to experimental data. These results show that the shear band width increases with the feed.

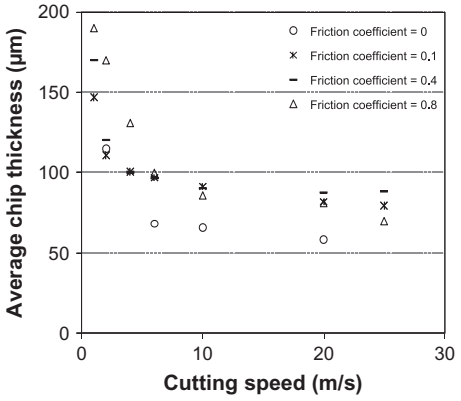

Fig. 13. Evolution of the average chip thickness with cutting speed for various values of the sliding friction coefficient (feed = 100 μm).

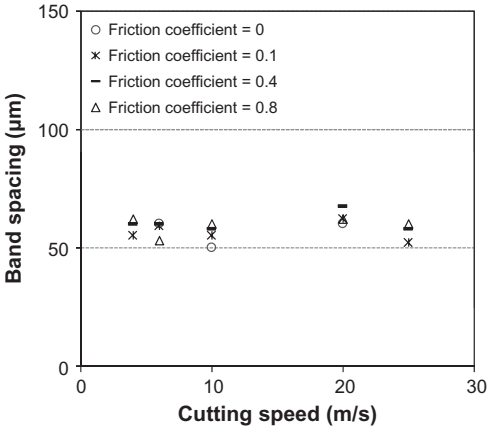

Fig. 14. Shear band spacing L_s in terms of the cutting speed for various values of the sliding friction coefficient (feed = 100 μm).

changing the level of the reference strain chosen in the definition of the shear band width.

The theoretical evolution of the shear band width with cutting speed is displayed in Fig. 12a (log–log diagram) for the feed f=0.1 mm. The two characterizations $w_{20\%}$ and $w_{10\%}$ show similar trends, i.e. a decreasing of the shear band width when the cutting speed is increased. The shear band width was measured in [6] for experiments at high cutting speeds (>10 m/s). Measures were easily made in this range of velocities since shear band boundaries were quite well defined (probably due to phase transformation within the shear zones).

The experimental data are compared against simulation results in Fig. 12a, and the agreement appears as reasonably good. In this log–log diagram, showing the shear band width versus cutting speed, a trend to the slope −1 is observed for experimental data and a similar tendency is seen for numerical simulations but to a lower extent.

The slope −1 corresponds to a shear band width being inversely proportional to the cutting speed (width~1/V). It should be noted that the later trend was theoretically predicted for adiabatic shear bands by Wright and Ockendon [36] and Dinzart and Molinari [37].

The decreasing of the width of adiabatic shear bands at higher shear rates can be explained as follows [36–38]. At higher strain rates, the heat produced by plastic flow within a given shear band has less time to be transferred to the surrounding by heat diffusion effects. This leads to a narrowing of the heat affected zone. Finally, noting that strain localization is controlled by thermal softening, it can be concluded that the shear band width is directly related to the thickness of the heat affected zone and is therefore decreasing at higher cutting speeds.

The influence of feed on band width is illustrated in Fig. 12b, where theoretical results obtained with the criterion $w_{20\%}$ are compared against experimental data. It is clearly observed from both numerical and experimental results, that the band width increases with feed.

5. Chip morphology: effect of friction and material parameters

5.1. Influence of the sliding friction coefficient

Fig. 13 shows the mean chip thickness $\bar{t}_2$ in terms of the cutting speed for the feed f = 100 μm and for various values of the sliding friction coefficient. It is seen that the chip thickness decreases with cutting speed.

Fig. 14 shows that the influence of friction coefficient on band spacing is negligible.

5.2. Influence of rheological parameters

The influence of material properties on shear flow instability is well established. Heat conductivity, strain hardening, material rate

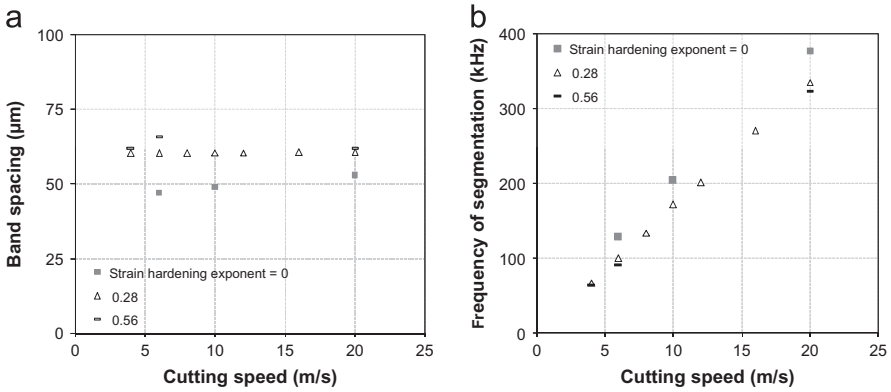

Fig. 15. (a) Shear band spacing L_s and (b) frequency of segmentation in terms of the cutting speed for various values of the strain hardening exponent n. L_s increases with n while the segmentation frequency decreases (stabilizing effect of strain hardening). The feed is equal to 100 μm.

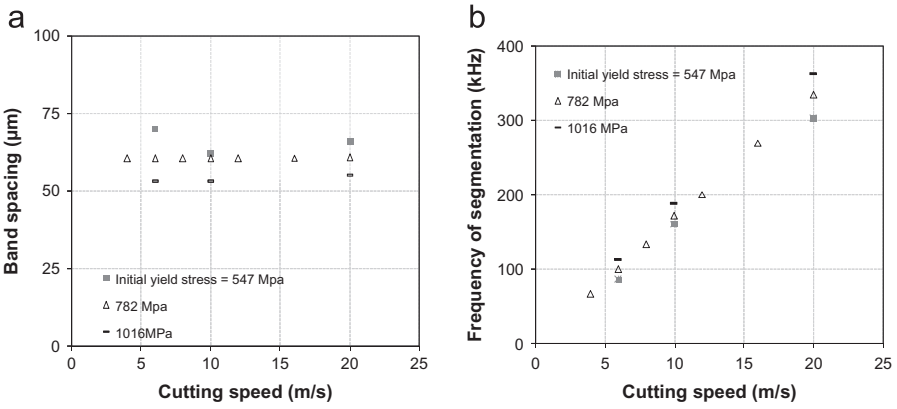

Fig. 16. (a) Shear band spacing L_s and (b) frequency of segmentation in terms of the cutting speed for various values of the initial yield stress A, Eq. (1). L_s decreases for higher values of A while the segmentation frequency increases. The feed is equal to 100 μm.

sensitivity and inertia have a stabilizing effect, while heat production and thermal softening have a destabilizing role as revealed by perturbation approaches and finite difference simulations, see for instance Molinari [39]. The effect on shear localization of strain softening (due to damage or phase transformation) and the role of initial geometrical defects, material heterogeneities and initial temperature fluctuations was investigated by Molinari and Clifton [40,41] based on a non-linear analytical approach. An overview of the role of material parameters and defects on adiabatic shear banding can be found in [42,43].

The effect of material parameters on the propagation of adiabatic shear bands was also investigated by analytical means by Mercier and Molinari [44] and with numerical modeling by Bonnet-Lebouvier et al. [45]. Similar effects were analyzed in [16] in the context of chip segmentation by adiabatic shearing.

In this section, we analyze the influence of the initial yield stress A and of the strain hardening exponent n of the constitutive law, Eq. (1). Fig. 15a and b shows the effect of the hardening exponent (n=0, 0.28, 0.56) on shear band spacing and segmenta-tion frequency. Increasing the value of n leads to larger band spacing. This is an expected outcome of the stabilizing effect of enhanced strain hardening [46]. The decreasing of the segmenta-tion frequency for higher values of the hardening exponent observed in Fig. 15b is simply a consequence of the enhanced shear band spacing. Otherwise, Fig. 15a and b confirms the insensitivity of the band spacing with respect to the cutting speed V and the linear dependence of the segmentation frequency with respect to V previously observed in Figs. 9 and 10.

In Fig. 16, the yield stress A is varied by +/−30% (resp. 547 MPa and 1016 MPa)) with respect to the reference value A=782 MPa given in Table 1. Increasing the level of the elastic limit, results in higher level of plastic work and of dissipated heat energy. Thus, the effect of thermal softening is enhanced and so is flow instability. Therefore, the increasing of A should lead to smaller shear band spacing and higher segmentation frequency. These features are indeed observed in the results displayed in Fig. 16a and b.

6. Conclusions

Adiabatic shear banding was analyzed with a numerical model developed in ABAQUS/explicit, able to reproduce shear localization phenomena involved in high speed machining of Ti6Al4V. The model was applied to the simulation of orthogonal cutting and was validated with theoretical and experimental works of the literature.

The conclusions that can be derived from this numerical study are four-fold.

Firstly, the effects of cutting conditions on chip segmentation were analyzed and it was demonstrated that:

- Shear band spacing does not depend upon cutting speed in the range of velocities explored here (1 m/s < V < 25 m/s).
- Segmentation frequency increases linearly with cutting speed for (1 m/s < V < 25 m/s), is inversely proportional to the feed and is not influenced by the value of the sliding friction coefficient.
- The width of shear adiabatic band is sensitive to cutting conditions, i.e. decreasing with higher cutting speeds and increasing with feed.

Secondly, effects of some material parameters on shear flow stability and chip morphology have been investigated

- As expected, the strain hardening exponent n has a stabilizing effect. By increasing n the band spacing is augmented and consequently, the segmentation frequency is decreased.
- Increasing the initial yield stress has a destabilizing effect that leads to smaller band spacing and higher segmentation frequency.

Thirdly, the effect of the sliding friction coefficient on chip segmentation and overall cutting forces has been analyzed

- The sliding friction coefficient has little effect on the shear band spacing
- For large values of the sliding friction coefficient ($\mu \geq 0.4$) the time averages of the cutting and thrust forces decrease significantly with the cutting speed V for $V \leq 5$ m/s and tend to limiting values at higher cutting speeds. These limits are independent of the values of μ.
- The overall friction coefficient follows similar trends.
- These features are due to the fact that sticking contact predominates at high cutting speeds when ($\mu \geq 0.4$). Then, the overall friction coefficient is mainly dependent upon the value of the flow stress of the work-material along the sticking zone. The results obtained here in the context of chip segmentation by adiabatic shearing generalize those derived in [2,21] in the context of continuous chip formation

Lastly, the correlation of the theoretical results with experimental data was found to be satisfactory.

Acknowledgments

The authors acknowledge the financial support of this work to the Ministry of Economy and Competitiveness of Spain with the project DPI2011-25999 and to the Universidad Carlos III de Madrid —Banco de Santander for the program ≪Chair of Excellence≫. This work was also supported by the French State through the program "Investment in the future" operated by the National Research Agency (ANR) and referenced by LabEx DAMAS.

Appendix A. Separation energy compared to cutting energy

The separation energy per unit time is given by: $W_{separation} = G_c b V$ where G_c is the separation energy per unit surface, b is the width of cut and V the cutting speed. The cutting energy is given by $W_{cutting} = F_{specific} b f_1 V$, where $F_{specific}$ is the specific cutting force. Thus, $W_{separation}/W_{cutting} = G_c/(F_{specific} f_1)$. A typical value of the specific cutting force for titanium is $F_{specific} = 1500\ N/\text{mm}^2$ and the separation energy was estimated in Section 2 as $G_c = 18,000\ J/m^2$. Thus, for the feed $f_1 = 100$ microns we have $W_{separation}/W_{cutting} = 0.12$.

Consequently, the separation energy plays a minor role as it appears to be small compared to the total cutting energy for values of the feed of about 100 microns and larger. It follows, that there is no necessity to precisely characterize the separation energy. A value of G_c broadly approaching $18,000\ J/m^2$ would be sufficient.

Let us check now that this condition is fulfilled. A rough estimate (lower bound estimate) of the separation energy involved in the proposed cutting model can be obtained from the work of plastic deformation within highly distorted elements in the process zone at the tip of the crack propagating along the machined surface. It appears that a layer of one element thickness is deleted in Zone B along the machined surface, according to the criterion $\varepsilon_{crit} = 3$. This corresponds to the path of the ductile crack that separates the chip from the workpiece. Above the machined surface, a layer with thickness of about three elements is highly deformed to a value of the strain close to 3. Below the crack a layer of two elements is less deformed to a level of about $\varepsilon = 0.4$. The plastic work per unit volume in the highly deformed elements can be estimated as $\sigma_Y \varepsilon_{crit} = 2400\ \text{MJ}/m^3$ if we consider that the yield stress for Ti alloys is about $\sigma_Y = 800$ MPa and that the accumulated plastic strain is close to the value $\varepsilon = 3$. Considering that the element size is $\delta = 1\ \mu m$, that a layer of 4 adjacent elements is highly deformed at the crack tip and neglecting the work of deformation in the elements below the crack, a lower bound of the plastic work associated to the propagation of the ductile crack is obtained as: $W_{layer} = 4\delta\sigma_Y\varepsilon_{crit} = 9600\ J/m^2$. This quantity corresponds to the separation energy per unit cutting width and per unit cutting length involved in the numerical model. It is seen that $W_{layer} = 9600\ J/m^2$ is smaller (lower bound) than the value of the separation energy for titanium alloys that was estimated as $G_c = 18,000\ J/m^2$. It can be noted that these values are of comparable magnitude.

The value of W_{layer} could be adjusted by tuning the element size δ. However, this is of no importance, since, as previously discussed, the contribution of the separation energy to the total cutting work remains small for titanium alloys and for the values of the feed considered in this work.

References

[1] Cantero JL, Tardío MM, Canteli JA, Marcos M, Miguélez MH. Dry drilling of alloy Ti6Al4V. Int J Mach Tools Manuf 2005;45:1246–55.
[2] Molinari A, Cheriguene R, Miguélez MH. Contact variables and thermal effects at the tool-chip interface in orthogonal cutting. Int J Solids Struct 2012;49:3774–96.
[3] Miguélez MH, Zaera R, Molinari A, Cheriguene R, Rusinek A. Residual stresses in orthogonal cutting of metals: the effect of thermomechanical coupling parameters and of friction. J Therm Stresses 2009;32:1–20.
[4] Hortig C, Svendsen B. Simulation of chip formation during high-speed cutting. J Mater Process Technol 2007;186:66–76.
[5] Hua J, Shivpuri R. Prediction of chip morphology and segmentation during the machining of titanium alloys. J Mater Process Technol 2004;150:124–33.
[6] Molinari A, Musquar C, Sutter G. Adiabatic shear banding in high speed machining of Ti–6Al–4V experiments and Modeling. Int J Plast 2002;18:443–59.
[7] Sun S, Brandt M, Dargusch MS. Characteristics of cutting forces and chip formation in machining of titanium alloys. Int J Mach Tools Manuf 2009;49:561–8.
[8] Cotterell M, Byrne G. Dynamics of chip formation during orthogonal cutting of titanium alloy Ti–6Al–4V. CIRP Ann-Manuf Technol 2008;57:93–6.
[9] Umbrello D. Finite element simulation of conventional and high speed machining of Ti6Al4V alloy. J Mater Process Technol 2008;196:79–87.
[10] Muñoz-Sánchez A, González-Farias IM, Soldani X, Miguélez MH. Hybrid FE/ANN and LPR approach for the inverse identification of material parameters from cutting tests. Int J Adv Manuf Technol 2011;54:21–33.
[11] Calamaz M, Coupard D, Girot F. A new material model for 2D numerical simulation of serrated chip formation when machining titanium alloy Ti–6Al–4V. Int J Mach Tools Manuf 2008;48:275–88.
[12] Sima M, Özel T. Modified material constitutive models for serrated chip formation simulations and experimental validation in machining of titanium alloy Ti–6Al–4V. Int J Mach Tools Manuf 2010;50:943–60.
[13] Karpat Y. Temperature dependent flow softening of titanium alloy Ti6Al4V: an investigation using finite element simulation of machining. J Mater Process Technol 2011;211:737–49.
[14] Chen G, Ren C, Yang X, Jin X, Guo T. Finite element simulation of high-speed machining of titanium alloy (Ti–6Al–4V) based on ductile failure model. Int J Adv Manuf Technol 2011;56:1027–38.
[15] Bäker M, Rösler J, Siemers C. A finite element model of high speed metal cutting with adiabatic shearing. Comput Struct 2002;80:495–513.
[16] Bäker M. Finite element investigation of the flow stress dependence of chip formation. J Mater Process Technol 2005;167:1–13.
[17] Bäker M, Rösler J, Siemers C. The influence of thermal conductivity on segmented chip formation. Comput Mater Sci 2003;26:175–82.
[18] Childs THC. Friction modeling in metal cutting. Wear 2006;260(3):310.
[19] Dixit US, Joshi SN, Davim JP. Incorporation of material behavior in modeling of metal forming and machining processes: a review. Mater Des 2011;32:3655.
[20] Muñoz-Sánchez A, Canteli JA, Cantero JL, Miguélez MH. Numerical analysis of the tool wear effect in the machining induced residual stresses. Simul Modelling Pract Theory 2011;19:872–86.

[21] Molinari A, Cheriguene R, Miguélez MH. Numerical and analytical modeling of orthogonal cutting: the link between local variables and global contact characteristics. Int J Mech Sci 2011;53:183–206.
[22] Hibbit, Karlson, Sorensen. ABAQUS User's Manual 6.4-1. 2003.
[23] Wierzbicki T, Bao Y, Lee Y-W, Bai Y. Calibration and evaluation of seven fracture models. Int J Mech Sci 2005;47:719–43.
[24] Rusinek A, Zaera R. Finite element simulation of steel ring fragmentation under radial expansion. Int J Impact Eng 2007;34:799–822.
[25] Johnson GR, Cook WH, A constitutive model and data for metals subjected to large strains, high strain rate and temperature. In: Proceedings of the 7th International Symposium of Ballistics, The Hague; 1983. p. 541–7.
[26] Lee W-S, Lin C-F. High-temperature deformation behaviour of Ti6Al4V alloy evaluated by high strain-rate compression tests. J Mater Process Technol 1998;75:127–36.
[27] ⟨www.azom.com⟩; [accessed January 2013].
[28] Armendia M, Garay A, Iriarte LM, Arrazola PJ. Comparison of the machinabilities of Ti6Al4V and TIMETAL® 54M using uncoated WC–Co tools. J Mater Process Technol 2010;210:197–203.
[29] Cotterell M, Byrne G. Characterization of chip formation during orthogonal cutting of titanium alloy Ti–6Al–4V. CIRP Ann-Manuf Technol 2008:81–5.
[30] Fang N, Wu Q, A comparative study of the cutting forces in high speed machining of Ti–6Al–4V and Inconel 718 with a round cutting edge tool. J Mater Process Technol 2009;209:4385–9.
[31] Hoffmeister, HW, Gente, A, Weber, T, Chip formation of titanium alloys.
In: Proceedings of 2nd International Conference on High Speed Machining. Darmstadt: Germany; 1999. p. 21–8.
[32] Gente A, Hoffmeister H-W. Chip formation in machining Ti6A14V at extremely high cutting speeds. CIRP Ann-Manuf Technol 2001;50(1):49–52.
[33] Osovski S, Rittel D, Landau P, Venkert A. Microstructural effects on adiabatic shear band formation. Scr Mater 2012;66:9–12.
[34] Ye GG, Xue SF, Jiang MQ, Tong XH, Dai LH. Modeling periodic adiabatic shear band evolution during high speed machining Ti–6Al–4V alloy. Int J Plast 2013;40:39–55.
[35] Atlati S, Haddag B, Nouari M, Zenasni M. Analysis of a new segmentation intensity ratio "SIR" to characterize the chip segmentation process in machining ductile metals. Int J Mach Tools Manuf 2011;51:687–700.
[36] Wright TW, Ockendon H. A model for fully formed shear bands. J Mech Phys Solids 1992;40:1217–26.
[37] Dinzart F, Molinari A. Structure of adiabatic shear bands in thermo-viscoplastic materials. Eur J Mech A/Solids 1998:923–38.
[38] Dodd B, Bai Y. Width of adiabatic shear bands. Mater Sci Tech 1985;1:38–40.
[39] Molinari A. Instabilité thermoviscoplastique en cisaillement simple. J de Méc Théor et Appl 1985;4(5):659–84.
[40] Molinari A, Clifton R. Localisation of the viscoplastic deformation in simple shear: exact results in non-linear theory. C R Acad des Sci, Paris, II 1983;296:1–4.
[41] Molinari A, Clifton R. Analytical characterization of shear localization. J Appl Mech 1987;54:806–912.
[42] Bai Y, Dodd B. Adiabatic shear localization. Oxford: Pergamon; 1992.
[43] Wright TW. The physics and mathematics of adiabatic shear bands. Cambridge: Cambridge Univ. Press; 2002.
[44] Mercier S, Molinari A. Steady-state shear band propagation under dynamic conditions. J Mech Phys Solids 1998;46:1463–95.
[45] Bonnet-Lebouvier AS, Molinari A, Lipinski P. Analysis of the dynamic propagation of adiabatic shear bands. Int J Solids Struct 2002;39:4249–69.
[46] Molinari A. Collective behavior and spacing of adiabatic shear bands. J Mech Phys Solids 1997;45(9):1551–73.